THE JOURNAL OF PHYSICAL CHEMISTRY Letters

Letter

pubs.acs.org/JPCL

Rotation of Four Small Nitroxide Probes in Supercooled Bulk Water

Ida Peric, Dalibor Merunka,† Barney L. Bales, and Miroslav Peric*

Department of Physics and Astronomy and The Center for Supramolecular Studies, California State University at Northridge, Northridge, California 91330, United States

Supporting Information

ABSTRACT: Using a precise method of least-squares nonlinear electron paramagnetic resonance (EPR) line fitting, we have obtained experimental evidence of a decoupling of the rotational motion of four nitroxide spin probes from the viscosity of bulk water at 277 K. This decoupling is about 50 K higher than another such phenomenon observed in interstitial supercooled water of polycrystalline ice by Banerjee et al. (*Proc. Natl. Acad. Sci. U.S.A.* **2009**, *106*, 11448−11453). Above 277 K, the activation energies of the rotation of the probes and the water viscosity are very close, while in the supercooled region, the activation energies of the probes' rotation are greater than that of the viscosity of water. The rotational correlation times of the probes can be fit well to a power law functionality with a singular temperature. The temperature dependence of the hydrodynamic radii of the probes indicates two distinct dynamical regions that cross at 277 K.

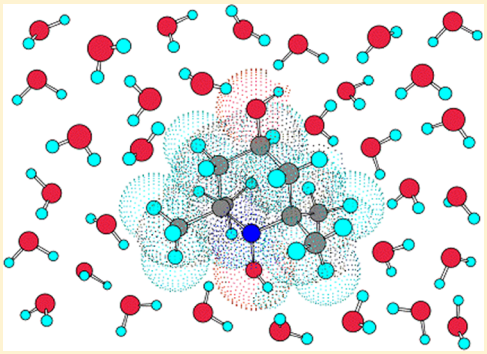

SECTION: Liquids; Chemical and Dynamical Processes in Solution

The importance and value of water are self-evident. Although water is an inorganic substance, it is at the same time "the most important organic molecule"; life as we know it is very likely impossible without water.[1] Water has amazing and unusual properties,[2−8] which makes it probably the most studied but still not completely understood substance.[8] Many fascinating phenomena in water occur when it is still in the liquid state below its melting point, in its supercooled state.[6] For example, the temperature behavior of the density, isothermal compressibility, thermal expansion coefficient, and isobaric heat capacity of supercooled water differ greatly from those of any simple liquid.

Recently, Banerjee et al.[9] have used electron paramagnetic resonance (EPR) spectroscopy to study the rotation of the small polar spin probe 4-hydroxy-2,2,6,6-tetramethylpiperidine-1-oxyl (TEMPOL) in deeply supercooled water, from 90 to 300 K. The rotation of TEMPOL revealed the coexistence of two liquid phases in that range, the Debye−Stokes−Einstein breakdown and the decoupling of the rotation of TEMPOL from the viscosity at 225 K. The EPR spectra of TEMPOL in rapid-quench-formed amorphous water taken by Bhat et al.[10] indicate that supercooled water coexists with crystalline (cubic) ice in the temperature range of 140−210 K, that is, in the so-called "no man's land (NML)". The glass transition temperature of water at ∼135 K was observed as a sharp reduction in the separation of the two outermost components of the EPR spectrum of TEMPOL (Figure 2 of ref 10). Banerjee et al. have also studied the dynamics of TEMPOL in strongly confined supercooled water.[11] The anomalous behavior of the rotation of the spin probe di-tert-butyl nitroxide (DTBN) in supercooled water was observed[12] and attributed to the local fluctuating structures, which were very likely connected to the water hydrogen bond network dynamics. Another study of the rotational motion of DTBN in EPR revealed that the EPR line widths of the probe increase rapidly with decreasing temperature below 0 °C due to the rapid increase of the viscosity of supercooled water.[13] The crystallization temperature of water can be lowered by subdividing the sample into small droplets;[6] therefore, quite often, water is encapsulated in small geometric confinements to study its properties in NML.[14] The spin probe EPR technique has been used to study supercooled water confined in a polyuria microcapsule[15] and a silica gel with high hydration level.[16]

The current work aims to carry out careful and precise EPR measurements of the rotational motion of four small nitroxide spin probes in bulk water in the temperature range of 253−363 K. Using a precise method of least-squares nonlinear EPR line fitting, we seek to learn if there is any difference in the rotational diffusion of the probes in the supercooled and normal regions.

The nitroxides used in this work were perdeuterated 2,2,6,6-tetramethylpiperidine-1-oxyl (pDT or pD-TEMPO), perdeuterated 4-oxo-2,2,6,6-tetramethylpiperidine-1-oxyl (pDTO or pD-TEMPONE), perdeuterated 4-hydroxy-2,2,6,6-tetramethylpiperidine-1-oxyl (pDTOH or pD-TEMPOL), and DTBN (Scheme 1); we will be using the shorter acronyms. pDT, pDTO, and pDTOH are nearly spherical molecules, whose van der Waals volumes are 170.4, 176.5, and 179.2 Å^3,[17] respectively, while DTBN is an ellipsoidal molecule with its major axis about 1.7 times longer than its minor axis[18] and a

Received: December 18, 2012
Accepted: January 18, 2013

   dx.doi.org/10.1021/jz302107x | *J. Phys. Chem. Lett.* 2013, 4, 508−513

Scheme 1. pDT, pDTO, pDTOH, and DTBN

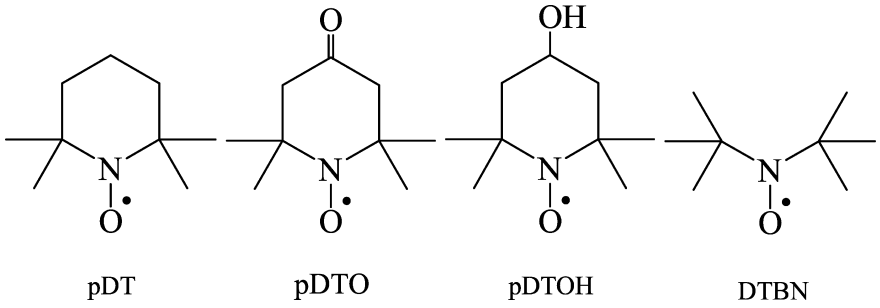

van der Waals volume of 171 Å^3;[17] note that van der Waals volumes are all within 5% of each other. The perdeuterated probes have been chosen because they have a smaller Gaussian content contribution[19] than their hydrogenated equivalents, for example, TEMPOL in refs 9 and 11. The smaller Gaussian content produces narrower EPR lines and thereby a higher signal-to-noise ratio. The water viscosity data are taken from refs 20, 21, and 22 and are well described by $\eta = 0.13895[(T/224.85) - 1]^{-1.6617} cP$; almost all experimental points are within 1% of the fit.

The concentrations of pDT (lot# C119P1), pDTO (lot# P607P2), and pDTOH (lot# P339P4), all from C/D/N isotopes, and DTBN (lot# 04911LO, Aldrich) in distilled water were about 100 μM. Note that this concentration is about 50 times lower than the concentration of TEMPOL in refs 9 and 10. This low concentration is necessary to avoid EPR line broadening and dispersion in the EPR spectrum due to Heisenberg spin exchange collisions and dipole−dipole interactions.[23] For the EPR measurements above 277 K, the solutions were housed in 50 μL capillaries (radius ≈ 450 μm), while below 277 K, 5 μL capillaries (radius ≈ 150 μm) were used. EPR measurements were carried out with a Bruker ESR 300E spectrometer equipped with a Bruker variable-temperature unit. The sample temperature was measured with a thermocouple whose tip was positioned at the top of the EPR cavity and was held stable within ±0.2 K. Samples were measured in a temperature range from 253 to 353 K in increments of 2 K below 283 K and in increments of 10 K above 283 K. At several temperatures between 261 and 303 K, both 5 and 50 μL samples of each probe were measured in order to ensure that they give the same result within the experimental error. At each temperature, the samples were equilibrated for at least 5 min to ensure uniform temperature throughout the sample. Five first-harmonic EPR spectra were acquired at each temperature, employing a sweep time of 84 s, microwave power of 5 mW, time constant of 20.5 ms, and modulation amplitudes of 0.2 G for pDTO and 0.285 G for the other probes. The acquired spectra were analyzed with the home-written computer program Lowfit, as detailed previously.[24,25]

Figure 1 shows a typical EPR spectrum of pDT at 293 K in the fast motional regime. The line shape of most nitroxide spin probes is inhomogeneous mostly due to unresolved proton/deuteron hyperfine structure and field modulation.[26,27] The inhomogeneously broadened EPR spin probe line can be described quite well by a Voigt line shape,[19] which is a Gaussian distribution of Lorentzian lines (see the Supporting Information). The Voigt line shape can closely be approximated by the sum of a Gaussian and Lorentzian.[19,28] This fact enables one to extract the Lorentzian line widths from the inhomogeneously

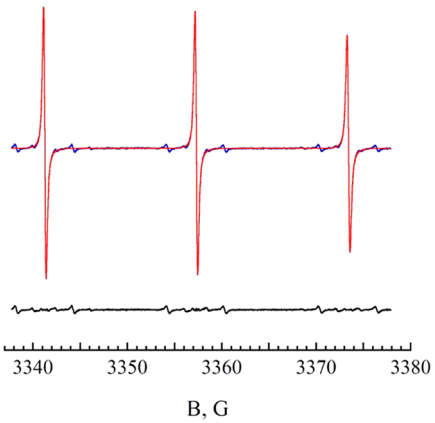

Figure 1. EPR spectrum of 100 μM pDT in water at 293 K (top blue trace). The fit of the spectrum (top red trace) is indistinguishable from the spectrum, except for the ^{13}C lines. The spectrum minus the fit gives the residual shown as the bottom trace.

broadened EPR lines using least-squares nonlinear EPR line fitting.[25,28−30] As can be seen in Figure 1, the fit of the experimental spectrum to the sum of a Gaussian and a Lorentzian is indistinguishable from the spectrum, except for the ^{13}C lines in the wings due to the natural abundance of ^{13}C in the probes. The peak-to-peak Lorentzian line width of an individual hyperfine line ΔB_m^L is given by[31,32]

$$\Delta B_m^L = A + Bm + Cm^2 \quad (1)$$

where m is the mth component of the nitrogen nuclear spin. Term A contains contributions other than motional and is the Lorentzian line width of the central line. Terms B and C are affected by the rotational motion of the probe as follows[31]

$$B = 0.103\omega_e[\Delta g \Delta A + 3(\delta g)(\delta A)]\tau_B\left(1 + \frac{3}{4}\frac{1}{1 + \omega_e^2\tau_B^2}\right) \quad (2)$$

$$C = 1.81 \times 10^6[(\Delta A)^2 + 3(\delta A)^2]\tau_C\left(1 - \frac{3}{8}\frac{1}{1 + \omega_N^2\tau_C^2} - \frac{1}{8}\frac{1}{1 + \omega_e^2\tau_C^2}\right) \quad (3)$$

where $\Delta A = A_{zz} - 1/2(A_{xx} + A_{yy})$, $\delta A = 1/2(A_{xx} - A_{yy})$, and A_{xx}, A_{yy}, and A_{zz} are the principal values of the hyperfine tensor. Similar expressions hold for the g tensor. $\omega_N = 8.8 \times 10^6 A_N$, where A_N is the isotropic hyperfine splitting and ω_e is the EPR spectrometer frequency. The g and A principal values that we used in our calculation are given in the Supporting Information.

dx.doi.org/10.1021/jz302107x | J. Phys. Chem. Lett. 2013, 4, 508−513

B and *C* values are found from the fits of the experimental data. Actually, instead of using the Lorentzian line widths to calculate the *B* and *C* values, we used the heights of the individual lines, which can be extracted from the spectrum with more precision. To account for the line shape effect on the relation between the line width and height, those values were then corrected according to the procedure described in ref 19. The corrected *B* and *C* values were then used in eqs 2 and 3 to find the rotational correlation times τ_B and τ_C. Uncorrected *B* and *C* values lead to errors up to 60% in τ_B and τ_C.[19] Our corrections reduce the errors to below 10%. Santangelo et al.[16] have shown that in the case of nearly spherical probes such as TEMPO in the fast motional regime ($\tau \leq 1$ ns), when the EPR line width is properly corrected for its Gaussian contribution, the line width method, eq 1, gives the rotational correlation time in very good agreement with that of a more rigorous simulation method, the EasySpin[33] function "chili", which is based on the stochastic Liouville equation.

Figure 2 shows the mean rotational correlation time, $\tau_R = (\tau_C\tau_B)^{1/2}$, of pDT, pDTO, pDTOH, and DTBN as a function

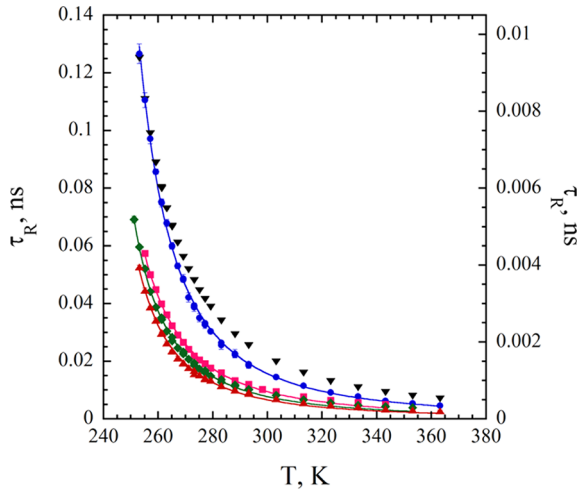

Figure 2. Rotational correlation time τ_R of pDTOH (circles), pDTO (squares), pDT (diamonds), and DTBN (triangles), left ordinate, and τ_R of water (inverted triangles) calculated using eq 2.4 from ref 34, right ordinate, as a function of temperature. The solid lines are fits to eq 4.

of temperature. In the same figure, the rotational correlation time of water measured by NMR from ^{17}O, calculated using eq 2.4 from ref 34, is presented. Although the rotation of pDTOH is about an order of magnitude slower than the rotation of water molecules, their functional dependence is very similar. The same is true for the other probes when their rotational correlation times are scaled to τ_R of water (see the Supporting Information). Due to the radii of the probes, about 3.5 Å, compared to that of a water molecule, 1.4 Å,[11] it is expected that the probes minimally modify their water environment. Each probe affects its surrounding slightly differently, which is reflected in the different values of τ_R. It appears that these four spin probes report well on the *changes* of the rotational diffusion of water, Figure 2. This implies that small, nearly spherical nitroxide probes are useful for studying supercooled water. The reason might be that the oxygen(s) of the nitroxides (Scheme 1) can contribute to hydrogen bonds with water.[35] The rotational motion of pDTOH is slower than that of the other probes. The most likely explanation for this is that because the OH moiety can also be involved in hydrogen bonding, pDTOH forms more hydrogen bonds than the other probes. The additional hydrogen bonds slow the rotation of pDTOH.[36,37] Also, note that our values for pDTOH are of the same order of magnitude as the one presented at the same temperature in Figure 4 in ref 9. The lines through the data are fits to the power law

$$\tau_R = \tau_{R0}\left(\frac{T}{T_0} - 1\right)^{-\gamma} \quad (4)$$

where τ_{R0} and γ are constants and T_0 is a thermodynamic singular temperature. Speedy and Angell[38] showed that eq 4 with $T_0 = 228$ K fits very well a variety of physical quantities; the value of γ was different for different quantities. It was also argued that in the case of transport properties, there could be the possible universality of the exponent, $\gamma \cong 2$.[14,39] The fit of the rotational correlation times to eq 4 with $\gamma = 2$ gives $T_0 = 228.1 \pm 0.3$ K (r, correlation factor = 0.999) for pDTOH, $T_0 = 224.3 \pm 0.4$ K ($r = 0.999$) for pDTO, $T_0 = 226.5 \pm 0.3$ K ($r = 0.999$) for pDT, and $T_0 = 227.0 \pm 0.4$ K ($r = 0.998$) for DTBN (Figure 2). Although all of these values are close to 228 K, we concur with Qvist et al.,[34] who caution against interpreting these parameters within the framework of mode-coupling theory. These fits show for the first time that the rotational motion of a small nitroxide probe in water can be described as many other physical properties of water[38] using eq 4. If the τ_R data and the viscosity of water η above and below 277 K are fit to the Arrhenius equation $\tau_{R0}\exp(E_A/RT)$ (Figure 3a and b), it can be observed that the activation energies of τ_R and η above 277 K are similar (Table 1). The activation energy of τ_R for pDTOH, 19.1 kJ/mol, is slightly greater than the activation energies for the other probes and the viscosity, which are about 16.0 kJ/mol. In other words, the rotations of pDT, pDTO, and DTBN are coupled to the viscosity. Interestingly, this activation energy is the same as the one measured for the inverse of self-diffusion of supercooled water below 225 K, 16.5 kJ/mol, by Chen et al.[40] The greater activation energy of τ_R for pDTOH is very likely caused by the larger number of hydrogen bonds with water molecules. Below 277 K, the data can be fitted much better by the super-Arrhenius equation $\tau_R = \tau_{R0}\exp[A/(T - T_C)]$, not shown here. In order to estimate the activation energies below 277 K, we fit the data to the Arrhenius equation. The activation energy of τ_R for all of the probes is much greater than that of the viscosity (Table 1). The greater activation energies could be explained by a contribution from thermally induced structural changes in the supercooled water.[34] These data seem to indicate a decoupling between the rotation of the probe molecules and the viscosity in bulk water at about 277 K.

The Stokes–Einstein–Debye (SED) equation is given by

$$\tau_R = \frac{4\pi r^3}{3}\frac{\eta}{kT} \quad (5)$$

where r is the hydrodynamic radius of the probe, which is usually different from the van der Waals radius r_{vdW}. The ratio $f = r/r_{vdW}$ goes from 0 for the perfectly slip boundary condition (BC) to 1 for the stick BC (hydrodynamic behavior). Thus, the value of the hydrodynamic radius indicates the BC[41] of the probe, which can reflect collisional effects[42] and/or molecular inhomogeneity[43] in the microscopic boundary layer about the rotating probe. The departure from the SED behavior can be observed as a change in slope in a plot of $\tau_R T/\eta$ versus T. Figure 4 shows such a plot for pDT, pDTO, pDTOH, and

dx.doi.org/10.1021/jz302107x | J. Phys. Chem. Lett. 2013, 4, 508–513

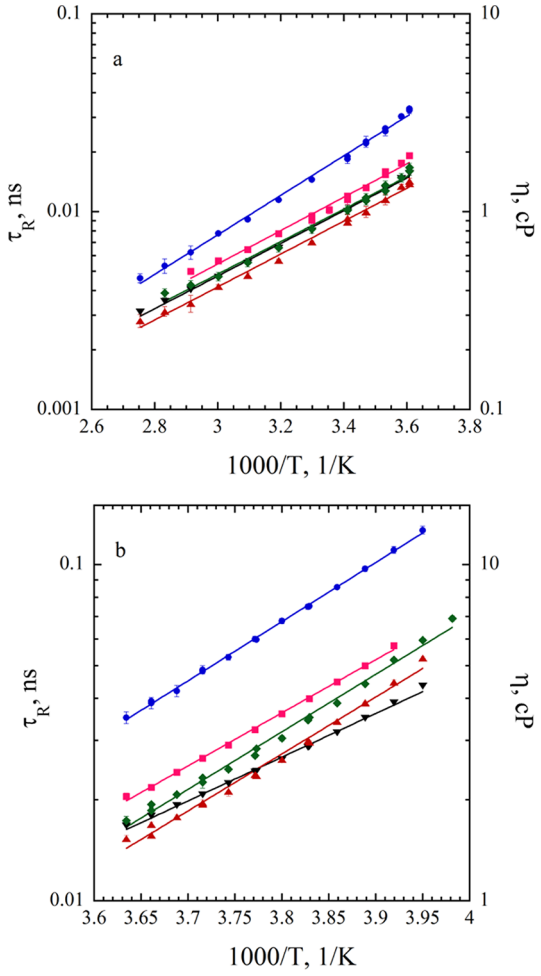

Figure 3. Rotational correlation time τ_R of pDTOH (circles), pDTO (squares), pDT (diamonds), and DTBN (triangles), left ordinate, and viscosity of water η (inverted triangles), right ordinate, as a function of the inverse of temperature; (a) above and (b) below 277 K. The solid lines are fits to the Arrhenius equation $\tau_{R0}\exp(E_A/RT)$; the correlation coefficients are 0.99 or greater.

Table 1. Activation Energies of the Rotation of pDT, pDTO, pDTOH, and DTBN and the Water Viscosity above and below 277 K

	E_a, kJ/mol (T > 277 K)	E_a, kJ/mol (T < 277 K)
τ_R pDT	15.7 ± 0.6	32.7 ± 0.7
τ_R pDTO	16.1 ± 0.6	30.9 ± 0.4
τ_R pDTOH	19.1 ± 0.5	33.8 ± 0.3
τ_R DTBN	15.9 ± 0.5	32.4 ± 0.8
η	15.8 ± 0.3	24.8 ± 0.5

DTBN. In Figure 4, we can clearly observe two distinct dynamical regions, one in the supercooled region and the other in the normal water region. For all of the probes, the temperature where the two regions cross can be estimated to be 277 ± 2 K, corresponding to the temperature where the rotational motion decouples from the viscosity. Again, pDTOH is slightly different from the other probes. In the normal region, the rotation of pDTOH follows the SED equation, while in the supercooled region, it does not. In the case of the other three probes, the rotation does not obey the SED equation in either region. In the supercooled temperature region, the slope of $\tau_R T/\eta$ is negative, clearly shown by all probes, while in the

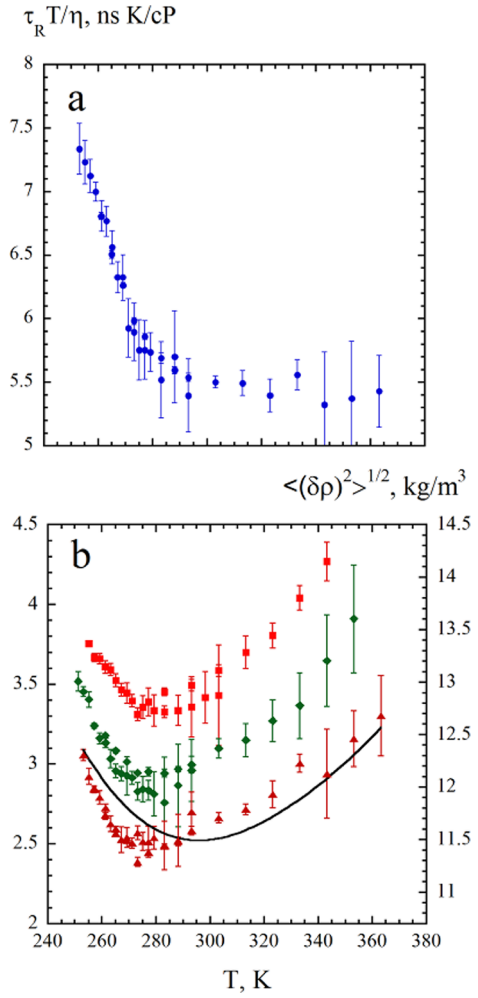

Figure 4. $\tau_R T/\eta$, left ordinate, for pDTOH (circles, a), pDTO (squares, b), pDT (diamonds, b), and DTBN (triangles, b) as a function of temperature. The solid line in (b) shows the density fluctuations $\langle(\delta\rho)^2\rangle^{1/2}$ in water assuming a sphere of radius 15 Å around the probe, right ordinate. Note that there are two data points for each probe at a few temperatures. The error bars are the standard deviations of five consecutive measurements.

normal water region, the slope is positive for pDT, pDTO, and DTBN and constant for pDTOH.

The rotational correlation time EPR measurements of pDT, pDTO, and DTBN in bulk water indicate that their rotational motion starts decoupling from the viscosity below 277 K. This conclusion has been possible due to a larger number of points in the measured temperature range of 255−353 K in this work compared with that in the previous studies[9,12,13] and by the use of probes producing narrow EPR lines. The power law increase in τ_R suggests that the probe rotation occurs in molecular cages, that is, the probe is confined by the formation of a strong network of tetrahedrally coordinated water molecules.[6,44,45] Because each probe molecule rotates in an ordered cage of water molecules and the size of this cage increases below and above 277 K, the rotation of the probe should be facilitated. According to Figure 4b, the effective hydrodynamic radius of the probe, eq 5, increases below and above 277 K; this can be interpreted as a slowing of the probe's rotation, if we assume that the SED equation is valid and the hydrodynamic radius measured at 277 K remains constant. The density fluctuations

dx.doi.org/10.1021/jz302107x | J. Phys. Chem. Lett. 2013, 4, 508−513

of a fixed number of moles in a volume V of a liquid are given by[46,47]

$$\langle(\delta\rho)^2\rangle = \langle\rho^2\rangle kT\kappa/V \quad (6)$$

where k is the Boltzmann constant and κ is the isothermal compressibility. Assuming that V is a sphere of radius 15 Å around the probe and using the data for ρ and κ from ref 48, we plot $\langle(\delta\rho)^2\rangle^{1/2}$ as a function of temperature in Figure 4b; the scale is adjusted so that the solid line overlaps with the $\tau_R T/\eta$ data for DTBN. As can be seen, the shapes of $\langle(\delta\rho)^2\rangle^{1/2}$ and $\tau_R T/\eta$ are similar. Therefore, possible reasons for the change in the hydrodynamic radius in the supercooled region can be an increase in hydrogen bonding between water molecules and the probe[49] and the increase in density fluctuations with decreasing temperature.[6,50] In the normal region, a likely reason for the increase in r could be the increase in density fluctuations with increasing temperature.[6,50] From the BC perspective, we have to consider what happens in the boundary layer around the probe. Kobryn et al.[51] have performed the theoretical study and numerical calculation of the rotation of methanol in water as a function of density/pressure, and they have found that the orientational relaxation time of methanol anomalously increases with increasing number density fluctuations or decreasing density below 1 g/cm^3. Note that the spin probes also form hydrogen bonds with water molecules as does methanol. Using the Kobryn et al. approach, we can propose a simple physical picture as follows: when the density fluctuations increase, the number of the collisions between the probe and water molecules in the boundary layer increases, which in turn could slow down the probe rotation due to an interplay between the collisional and dielectric frictions. The dielectric friction is produced by the inhomogeneity in the charge density of water, caused by the density fluctuation due to the hydrogen bond.[51] In other words, the BC becomes less slip; therefore, the hydrodynamic radius appears larger (Figure 4).

The van der Waals radius is 3.43 Å for pDT, 3.48 Å for pDTO, 3.50 Å for pDTOH Å, and 3.44 Å for DTBN. Although its van der Waals radius is not any different, pDTOH behaves somewhat differently than the other probes; (i) τ_R of pDTOH is about double that for the other probes, (ii) the activation energy of τ_R is greater by about 3.0 kJ/mol in the normal region, and (iii) the hydrodynamic radius of pDTOH is greater at 277 K (2.6 Å compared to 2.2 Å (pDTO), 2.1 Å (pDT), and 2.0 Å (DTBN)), and it increases two times faster than those of the other probes in the supercooled region (Figure 4). These differences are due to the OH moiety, which is more effective in hydrogen bonding than the N−O. moiety.

■ ASSOCIATED CONTENT

Ⓢ Supporting Information

Figures of the rotational times of probes and water, Voigt line shape, g and A tensor principal values, and Gaussian line width values. This material is available free of charge via the Internet at http://pubs.acs.org.

■ AUTHOR INFORMATION

Corresponding Author

*E-mail: miroslav.peric@csun.edu.

Present Address

†D.M.: Ruder Boskovic Institute, Zagreb, Croatia.

Notes

The authors declare no competing financial interest.

■ ACKNOWLEDGMENTS

D.M. and M.P. gratefully acknowledge support from NIH Grant 1 SC3 GM099635-01.

■ REFERENCES

(1) Alberts, B.; Bray, D.; Lewis, J.; Raff, M.; Roberts, K.; Watson, J. D. *Molecular Biology of the Cell*; 3rd ed.; Garland Publishing, Inc.: New York, 1994.

(2) Debenedetti, P. A.; Stanley, H. E. Supercooled and Glassy Water. *Phys. Today* **2003**, *56*, 40−46.

(3) Angell, C. A. Insights into Phases of Liquid Water from Study of Its Unusual Glass-Forming Properties. *Science* **2008**, *319*, 582−587.

(4) Mishima, O.; Stanley, H. E. The Relationship between Liquid, Supercooled and Glassy Water. *Nature* **1998**, *396*, 329−335.

(5) Angell, C. A. Amorphous Water. *Annu. Rev. Phys. Chem.* **2004**, *55*, 559−583.

(6) Debenedetti, P. A. Supercooled and Glassy Water. *J. Phys.: Condens. Matter* **2003**, *15*, R1669−R1726.

(7) Nilsson, A.; Pettersson, L. G. M. Perspective on the Structure of Liquid Water. *Chem. Phys.* **2011**, *389*, 1−34.

(8) Teixeira, J. Recent Experimental Aspects of the Structure and Dynamics of Liquid and Supercooled Water. *Mol. Phys.* **2012**, *110*, 249−258.

(9) Banerjee, D.; Bhat, S. N.; Bhat, S. V.; Leporini, D. ESR Evidence for 2 Coexisting Liquid Phases in Deeply Supercooled Bulk Water. *Proc. Natl. Acad. Sci. U.S.A.* **2009**, *106*, 11448−11453.

(10) Bhat, S. N.; Sharma, A.; Bhat, S. V. Vitrification and Glass Transition of Water: Insights from Spin Probe ESR. *Phys. Rev. Lett.* **2005**, *95*, 235702/1−235702/4.

(11) Banerjee, D.; Bhat, S. N.; Bhat, S. V.; Leporini, D. Molecular Probe Dynamics Reveals Suppression of Ice-Like Regions in Strongly Confined Supercooled Water. *PLoS ONE* **2012**, *7*, e44382(44388).

(12) Floridi, G.; Lamanna, R.; Cannistraro, S. Rotational Dynamics of Di-tert-butyl-nitroxide in Normal and Supercooled Water. *Appl. Magn. Reson.* **1994**, *7*, 537−550.

(13) Ahn, M.-K. Electron Spin Relaxation of Di-tert-butyl Nitroxide in Supercooled Water. *J. Chem. Phys. B* **1976**, *64*, 134−138.

(14) Mallamace, F.; Branca, C.; Corsaro, C.; Leone, N.; Spooren, J.; Stanley, H. E.; Chen, S.-H. Dynamical Crossover and Breakdown of the Stokes−Einstein Relation in Confined Water and in Methanol−Diluted Bulk Water. *J. Phys. Chem. B* **2010**, *114*, 1870−1878.

(15) Yamane, H.; Ohshima, H.; Kondo, T. Freezing Behaviour of Microencapsulated Water. *J. Microencapsulation* **1992**, *9*, 279−286.

(16) Santangelo, M. G.; Levantino, M.; Cupane, A.; Jeschke, G. Solvation of a Probe Molecule by Fluid Supercooled Water in a Hydrogel at 200 K. *J. Phys. Chem. B* **2008**, *112*, 15546−15553.

(17) Zhao, Y. H.; Abraham, M. H.; Zissimos, A. M. Fast Calculation of van der Waals Volume as a Sum of Atomic and Bond Contributions and Its Application to Drug Compounds. *J. Org. Chem.* **2003**, *68*, 7368−7373.

(18) Katter, U. J.; Hill, T.; Risse, T.; Schlienz, H.; Beckendorf, M.; Klüner, T.; Hamann, H.; Freund, H.-J. Dynamics of the Stable Radical Di-tert-butyl Nitroxide on an Epitaxially Grown Al_2O_3 Film. *J. Chem. Phys. B* **1997**, *101*, 3776−3780.

(19) Bales, B. L. In *Spin Labeling: Theory and Applications*; Berliner, J. L., Reuben, J., Eds.; Plenum: New York, 1989; Vol. 8, pp 77−130.

(20) Cho, C. H.; Urquidi, J.; Singh, S.; Robinson, G. W. Thermal Offset Viscosities of Liquid H_2O, D_2O, and T_2O. *J. Phys. Chem. B* **1999**, *103*, 1991−1994.

(21) Hallett, J. The Temperature Dependence of the Viscosity of Supercooled Water. *Proc. Phys. Soc.* **1963**, *82*, 1046−1050.

(22) Eicher, L. D.; Zwolinski, B. J. High-Precision Viscosity of Supercooled Water and Analysis of the Extended Range Temperature Coefficient. *J. Phys. Chem.* **1971**, *75*, 2016−2024.

(23) Peric, M.; Bales, B. L.; Peric, M. EPR Line Shifts and Line Shape Changes Due to Heisenberg Spin Exchange and Dipole−Dipole Interactions of Nitroxide Free Radicals in Liquids: 8. Further

Experimental and Theoretical Efforts to Separate the Effects of the Two Interactions. *J. Phys. Chem. A* **2012**, *116*, 2855−2866.
(24) Bales, B. L.; Peric, M. EPR Line Shifts and Line Shape Changes Due to Spin Exchange of Nitroxide Free Radicals in Liquids. *J. Phys. Chem. B* **1997**, *101*, 8707−8716.
(25) Bales, B. L.; Peric, M. EPR Line Shifts, and Line Shape Changes Due to Spin Exchange of Nitroxide Free Radicals in Liquids 2. Extension to High Spin Exchange Frequencies and Inhomogeneously Broadened Spectra. *J. Phys. Chem. A* **2002**, *106*, 4846−4854.
(26) Peric, M.; Halpern, H. J. Fitting of the Derivative Voight ESR Line under Conditions of Modulation Broadening. *J. Magn. Reson.* **1994**, *A 109*, 198−202.
(27) Bales, B. L.; Peric, M.; Lamy-Freund, M. T. Contributions to the Gaussian Line Broadening of the Proxyl Spin Probe EPR Spectrum Due to Magnetic-Field Modulation and Unresolved Proton Hyperfine Structure. *J. Magn. Reson.* **1998**, *132*, 279−286.
(28) Halpern, H. J.; Peric, M.; Yu, C.; Bales, B. L. Rapid Quantitation of Parameters from Inhomogeneously Broadened EPR Spectra. *J. Magn. Reson., Ser. A* **1993**, *103*, 13−22.
(29) Smirnov, A. I.; Belford, R. I. Rapid Quantitation from Inhomogeneously Broadened EPR Spectra by a Fast Convolution Algorithm. *J. Magn. Reson.* **1995**, *A 113*, 65−73.
(30) Robinson, B. H.; Mailer, C.; Reese, A. W. Linewidth Analysis of Spin Labels in Liquids; I Theory and Data Analysis. *J. Magn. Reson.* **1999**, *138*, 199−209.
(31) Schreier, S.; Polnaszek, C. F.; Smith, I. C. P. Spin Labels in Membranes Problems in Practice. *Biochim. Biophys. Acta* **1978**, *515*, 375−436.
(32) *EPR and Advanced EPR Study of Biological Systems*; Dalton, L. R., Ed.; CRC Press: Boca Raton, FL, 1984.
(33) Stoll, S.; Schweiger, A. EasySpin, A Comprehensive Software Package for Spectral Simulation and Analysis in EPR. *J. Magn. Reson.* **2006**, *178*, 42−55.
(34) Qvist, J.; Mattea, C.; Sunde, E. P.; Halle, B. Rotational Dynamics in Supercooled Water from Nuclear Spin Relaxation and Molecular Simulations. *J. Chem. Phys.* **2012**, *136*, 204505.
(35) Owenius, R.; Engström, M.; Lindgren, M.; Huber, M. Influence of Solvent Polarity and Hydrogen Bonding on the EPR Parameters of a Nitroxide Spin Lable Studied by 9-GHz and 95-GHz EPR Spectroscopy and DGT Calculations. *J. Phys. Chem. A* **2001**, *105*, 10967−10977.
(36) Hall, D. B.; Hamilton, K. E.; Miller, R. D.; Torkelson, J. M. Translational and Rotational Diffusion of Probe Molecules in Polymer Films near T_g: Effect of Hydrogen Bonding. *Macromolecules* **1999**, *32*, 8052−8058.
(37) Dutt, G. B. Molecular Rotation as a Tool for Exploring Specific Solute−Solvent Interactions. *Chem. Phys. Chem.* **2005**, *6*, 413−418.
(38) Speedy, R. J.; Angell, C. A. Isothermal Compressibility of Supercooled Water and Evidence for a Thermodynamic Singularity at −45°C. *J. Chem. Phys.* **1976**, *65*, 851−858.
(39) Elmatad, Y. S.; Chandler, D.; Garrahan, J. P. Corresponding States of Strutural Glass Formers; [cond-mat.stat-mech] 2008(arXiv:0811.2450v1).
(40) Chen, S. H.; Mallamace, F.; Mou, C.-Y.; Broccio, M.; Corsaro, C.; Faraone, A.; Liu, L. The Violation of the Stokes−Einstein Relation in Supercooled Water. *Proc. Natl. Acad. Sci. U.S.A.* **2006**, *103*, 12974−12978.
(41) Hu, C.-M.; Zwanzig, R. Rotational Friction Coefficients for Spheroids with the Slipping Boundary Condition. *J. Chem. Phys.* **1974**, *60*, 4354−4357.
(42) Hynes, J. T.; Kapral, R.; Weinberg, M. Molecular Rotation and Reorentation: Microscopic and Hydrodynamic Contributions. *J. Chem. Phys.* **1978**, *69*, 2725−2733.
(43) Dote, J. L.; Kivelson, D.; Schwartz, R. N. A Molecular Quasi-Hydrodynamic Free-Space Model for Molecular Rotational Relaxation in Liquids. *J. Phys. Chem.* **1981**, *85*, 2169−2180.
(44) Sciortino, F. Slow Dynamics in Supercooled Water. *Chem. Phys.* **2000**, *258*, 307−314.
(45) Sciortino, F.; Gallo, P.; Tartaglia, P.; Chen, S.-H. Supercooled Water and the Kinetic Glass Transition. *Phys. Rev. E* **1996**, *54*, 6331−6343.
(46) Callen, H. B.; John Wiley and Sons: New York, 1985.
(47) Ediger, M. D. Can Density or Entropy Fluctuations Explain Enhanced Translational Diffusion in Glass-forming Liquids? *J. Non-Cryst. Solids* **1998**, *235−237*, 10−18.
(48) *CRC Handbook of Chemistry and Physics*; Weast, R. C., Ed.; CRC Press: Cleveland, OH, 1977.
(49) Sastry, S.; Debenedetti, P. A.; Sciortino, F.; Stanley, H. E. Singularity-Free Interpretation of the Thermodynamics of Supercooled Water. *Phys. Rev. E* **1996**, *53*, 6144−6154.
(50) Xie, Y.; Ludwig, K. F.; Morales, G.; Hare, D. E.; Sorensen, C. M. Noncritical Behavior of Density Fluctuations in Supercooled Water. *Phys. Rev. Lett.* **1993**, *71*, 2050−2053.
(51) Kobryn, A. E.; Yamaguchi, T.; Hirata, F. Site−Site Memory Equation Approach in Study of Density/pressure Dependence of Translational Diffusion Coefficient and Rotational Relaxation Time of Polar Molecular Solutions: Acetonitrile in Water, Methanol in Water, and Methanol in Acetonitrile. *J. Chem. Phys.* **2005**, *122*, 184511.